Spatial and Fourier-space distribution of confined optical Tamm modes

Fu Feng, Willy Daney de Marcillac, Xavier Lafosse, Simone Luca Portalupi, Michel Nasilowski, Benoît Dubertret, Jean-Marc Frigerio, Catherine Schwob, Agnès Maître, Pascale Senellart, et al.

Spatial and Fourier-space distribution of confined optical Tamm modes

2016 New J. Phys. 18 083018

(http://iopscience.iop.org/1367-2630/18/8/083018)

New Journal of Physics
The open access journal at the forefront of physics

Deutsche Physikalische Gesellschaft DPG
IOP Institute of Physics

Published in partnership with: Deutsche Physikalische Gesellschaft and the Institute of Physics

OPEN ACCESS

RECEIVED
6 April 2016

REVISED
23 June 2016

ACCEPTED FOR PUBLICATION
14 July 2016

PUBLISHED
3 August 2016

PAPER

Spatial and Fourier-space distribution of confined optical Tamm modes

Fu Feng[1], Willy Daney de Marcillac[1], Xavier Lafosse[2], Simone Luca Portalupi[2], Michel Nasilowski[3], Benoît Dubertret[3], Jean-Marc Frigerio[1], Catherine Schwob[1], Agnès Maître[1], Pascale Senellart[2] and Laurent Coolen[1]

[1] Sorbonne Universités, UPMC Univ Paris 06, CNRS-UMR 7588, Institut des NanoSciences de Paris, F-75005, Paris, France
[2] Laboratoire de Photonique et de Nanostructures, CNRS UPR20, Route de Nozay, F-91460 Marcoussis, France
[3] Laboratoire de Physique et d'Etude des Matériaux, ESPCI, UPMC Univ Paris 6, CNRS, 10 rue Vauquelin, Paris, France

E-mail: feng@insp.jussieu.fr

Keywords: colloidal nanocrystals, optical mode Tamm, emission dispersion relation, fluorescence

Supplementary material for this article is available online

Abstract

In this paper, we characterize the electric field distribution of confined optical modes in a 0D Tamm structure, consisting in a metallic disk deposited on a Bragg mirror. The modes are probed at room temperature, through the fluorescence of semiconductor colloidal nanocrystals. We perform a combined analysis of the resonant modes distribution in both direct space and Fourier space and show, in good agreement with numerical simulations, that a subportion of the structure will radiate with a different angular distribution depending on its position. Such analysis is shown to probe the gradient of the phase of the confined optical modes.

1. Introduction

Manipulating light emission and propagation inside nanophotonics structures requires a fine understanding of the characteristics of their electromagnetic modes, such as their spectral properties, their spatial distribution, or the far-field angular radiation pattern. For instance, numerous studies have considered double Bragg reflector (DBR) micropillar optical cavities : some studies combined spatial and spectral analysis in order to map the spatial electric-field distribution of each optical mode [1–4], while other studies on micropillars (as well as photonic-crystal cavities, microdisks etc) combined spectral and far-field angular analysis in order to probe the radiation pattern of each optical mode [5, 6].

In this paper, we report the spectroscopic analysis of the electromagnetic modes excited in a 0D optical Tamm structure, with both spatial and angular resolutions : we select the field radiated from a sub-portion of the structure and image its radiation pattern. Such a measurement raises difficulties as the far-field radiation pattern is associated with the Fourier transform (k-vector distribution) of the structure electric-field spatial distribution [7], so that the photonic modes spatial distribution and angular (k-vector) distribution cannot be probed simultaneously wih unlimited precision. We find that the radiation pattern depends on the position of the probed sub-portion of the photonic structure. The agreement between measurement and simulation shows that the precision of simultaneous spatial and k-vector measurement is limited only, as expected, by diffraction.

The modes under study are optical Tamm modes, excited at room temperature by fluorescent colloidal nanocrystals. Optical Tamm modes are electromagnetic states confined at the interface between a DBR and a metallic film [8, 9]. They allow a direct coupling to far-field photonic modes, in both tranverse-electric and transverse-magnetic polarizations [10], while for surface plasmon-polaritons far-field radiation must be ensured, for instance, by a grating [11, 12]. If a metallic disk of micrometric diameter is deposited on a DBR, the Tamm state can be confined beneath the metallic disk [13], providing three-dimensional confinement with versatile fabrication methods. Coupling of such 0D Tamm structures to epitaxial quantum dots has been demonstrated at cryogenic temperature, leading to bright single-photon sources [14], enhanced fluorescence

[15] and low-threshold polarized nanolasers [16, 17]. Tamm states have also been proposed for other applications such as transparent contacts [18], photovoltaics [19] or biological detection [10].

The paper is organized as follows : in the second section, we describe, as a preliminary, the structure of samples with a DBR covered by a planar metallic layer (which we refer to as '2D Tamm' structures) or a metallic disk ('0D Tamm' structures) and the characterization of the optical Tamm modes dispersion relation. In the third section, we measure the electric field spatial and angular distribution by probing the k-vector and spectral properties from a portion of the disk and compare the results with numerical simulations. In the fourth section, we discuss this measurement and show how it provides a probe of the phase distribution of the modes complex electric field (while standard imaging provides only the electric field norm).

2. 2D and 0D Tamm structures

The Tamm structure[4] consists in a TiO_2/SiO_2 DBR (seven $\lambda/4$ pairs, last SiO_2 layer of thickness 89 nm) centered at $E = 1.94$ eV ($\lambda = 640$ nm) covered by a dense layer of CdSe/CdS core-shells nanocrystals (emission wavelength 640 nm [20]), then 60 nm of PMMA and a 55 nm layer of SiO_2. The PMMA layer (same optical index as SiO_2) prevents nanocrystals from being oxidized and damaged during silica deposition. The SiO_2 thicknesses are chosen to tune the Tamm wavelength in resonance with the nanocrystals emission and so that the nanocrystals are, in the z-direction, at the maximum of the Tamm state electric field. A 45 nm silver layer (for the 2D Tamm structure) or silver disks with 45 nm thickness and diameters from 1 to 10 μm (0D Tamm—see figure 2(a)) are then evaporated on top and covered by a protective 50 nm PMMA layer. For the 0D-Tamm structure, the disks were obtained by optical lithography. No lift-off was performed to remove the remaining photoresist: keeping the silver and resist layers around the silver disk does not change the Tamm mode structure, which is localized under the disk (see footnote 4), and allows masking the emission from nanocrystals that are not under the disk, which would otherwise hide the 0D-Tamm radiation.

As a first microphotoluminescence characterization, the sample was excited by a continuous laser (470 nm, 700 μW), focused by an objective with 0.7 numerical aperture (the measured laser spot size is about 1 μm). The emission was collected by the same objective and analyzed by a spectrometer coupled with a CCD camera. The rear focus plane of the objective (Fourier plane of the sample) was imaged onto the entrance slit of the spectrometer (figure 1(a)), so that the image on the camera yields analysis of the emitted light as a function of its energy E and its wavevector x-component k_x (which is related to the angle of emission θ by $k_x = (2\pi/\lambda)\sin\theta$).

Figure 1(b) shows the emission dispersion relation $E(k_x)$ for the 2D Tamm structure. This curve is characteristic of the 2D Tamm modes, with no direct emission from the nanocrystals not coupled to the Tamm modes, demonstrating the good coupling of the fluorescent nanocrystals to the Tamm modes. This measurement is in agreement with the $E(k_x)$ relation obtained by reflectometry (see footnote 4), shown by red dots on figure 1(b), confirming emission in the Tamm state. There is a slight 0.08 eV shift with respect to the simulations (see footnote 4) due to the imperfect control of sample layers thicknesses and the quality factor of the sample (90) is lower than simulated (200).

Figure 1(c) plots the same $E(k_x)$ dispersion relations for the 0D Tamm structures with different disk diameters. Again, the nanocrystals emission occurs only into the Tamm state. The emission from the 10 μm disk appears similar to the 2D case, with a parabolic curve starting at 1.97 eV. When the disk diameter is smaller than 6 μm, the higher energy part of the dispersion relation becomes less intense due to the confinement effect. For the 4 μm disk, a discrete mode begins to appear. For the 2 μm disk, this mode is blueshifted by 12 meV (4 nm) with respect to the 4 μm disk due to the Tamm state confinement. Note that we also observe emission from the sample area outside the disk forming an optical cavity constituted by the silica and photoresist layers between the DBR and the silver layer (parabolic curve above 2.07 eV and top of a parabolic curve below 1.98 eV).

3. Combined spatial and angular distributions of the 0D Tamm structure modes

In order to combine spatial and directional and spectral characterization of the emission, a motorized 100 μm pinhole was added in the image plane of the sample (figure 1(a)) in order to select emission originating from a 1.7 μm (given the $\times 60$ magnification between sample and image plane (figure 2(a))) portion of the sample surface. The pinhole was translated in the image plane so that the emission from different portions on the disk surface were considered seperately. The excitation laser spot, on the other hand, was kept at the center of the disk. Let us point out that spatial selection by the pinhole inevitably introduces diffraction, leading to a broadening of the radiation pattern by a cone of half-width $0.61\,\lambda/R = 0.22$ rad $= 12°$ (with $R = 0.85$ μm). An improvement of the spatial resolution, by using a sharper pinhole, would be at the cost of a reduced k-space

[4] See supplemental material at stacks.iop.org/NJP/18/083018/mmedia for sample fabrication details and support simulation details.

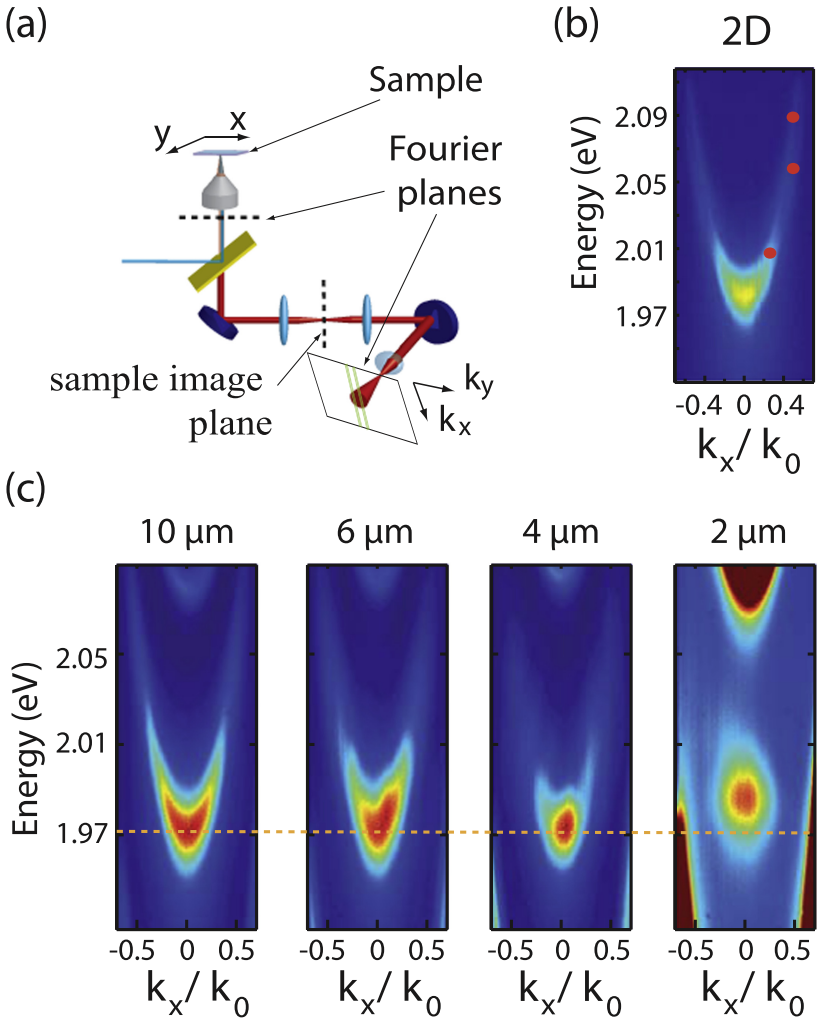

Figure 1. (a) Schematic experimental set-up. An image of the sample is formed in the image plane, where one can add a pinhole in order to select emission from a portion of the sample surface (section 3). The sample Fourier plane is imaged onto the entrance slit of a spectrometer in order to provide the k_x-vector and spectral resolutions. (b) Measured dispersion relation of the 2D Tamm ; the red dots are obtained from reflectometry data (see footnote 4). (c) Measured dispersion relation of 0D Tamm structure with different disk diameters. The dotted line indicates the energy of the fundamental mode for a 10 μm disk.

resolution. Our choice of 1.7 μm spatial resolution constitutes a good compromise as it allows us to evidence, on these structures, different k-space patterns depending on the probed position, as will be shown below.

The Tamm modes dispersion relations for detection positions $x = 0, \pm 2$ μm on the 10 μm disk are plotted in figure 2(a). When detection is performed at the center of the silver disk, the emission pattern is symmetric with a maximum intensity at $k_x = 0$ (it is not perfectly symmetric due to imperfect positioning of the pinhole at the center of the disk). When the detection position is shifted with respect to the disk center (at $x = -2$ μm and $x = +2$ μm), the emission pattern is no longer symmetric and has its maximum intensity at $k_x < 0$ and $k_x > 0$ respectively.

The structure was simulated using a finite elements method, with the $7(TiO_2/SiO_2)$/Ag layer thicknesses as defined previously and the structure covered by a 50 nm PMMA layer. In order to describe the fact that the emitting nanocrystals are the ones inside the excitation laser spot, which is of diffraction-limited diameter, we place 11 point sources respectively at $x = -500, -400 \ldots 400$ and 500 nm from the disk axis, with an oscillator strength decreasing with $|x|$ as a Gaussian of standard deviation 1 μm. In order to take into account the spectral shift between the designed and obtained structures, we express the wavelengths for simulations and experiments by their energy difference $\Delta E = E - E(k_x = 0)$, with the fundamental $E(k_x = 0) = 1.90$ eV (=652 nm) for the simulation and 1.98 eV (=625 nm) for the experiment.

The emitted electric field distribution is plotted at two different wavelengths in figure 2(b). The fundamental mode shows a single lobe at the center of the cavity, while several electric field maxima are observed for the higher-energy mode, corresponding to higher k_x components in the electric field distribution. For both modes, the emission (indicated by pink arrows normal to the wavefronts) is directed normal to the sample plane

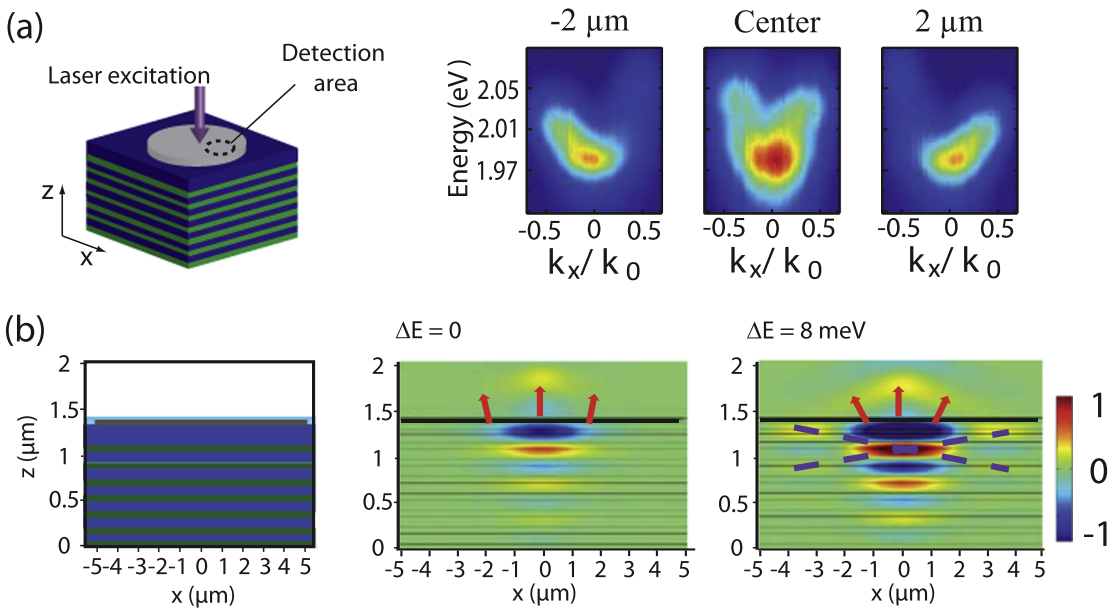

Figure 2. (a) Measured dispersion relation for detection areas at $x = -2$ μm, 0 and $+2$ μm on a 10 μm disk. (b) Finite elements simulation of the field distribution E_x at $\Delta E = 0$ and 8 meV (in 2D plane with y invariance ; we display here a 2×10.2 μm^2 portion of the full simulated cell, which was 2.4×20 μm^2 and surrounded by perfectly-matched layers). The black line shows the position of the silver disk and the pink arrows indicate the wave front propagation directions.

($k_x = 0$) on the disk axis ($x = 0$), while it is directed leftward on the left portion of the disk, and rightward on the right portion of the disk. The 8 meV simulation also shows clearly the relation between the outgoing wavefronts direction and the alignment of the mode lobes inside the structure (purple dotted lines). These simulation results are in agreement with the trend observed experimentally in figure 2(a): of the two modes centered at $k_x < 0$ and at $k_x > 0$ observed in figure 1(c), the mode centered at $k_x < 0$ is situated mostly in the $x < 0$ portion of the disk while the mode centered at $k_x > 0$ is located mostly in the $x > 0$ portion of the sample. Similar patterns (not shown here) were observed at $x = \pm 1$ and 3 μm. For $x = 0$, figure 2(a), shows that the emission is a lobe centered at $k_x = 0$.

For further quantitative analysis, figure 3(a) shows the measured and simulated radiation pattern at $\Delta E = 8$ and 25 meV over the collected numerical aperture. The simulated and measured patterns are in overall good agreement. For both cases, the intensity of emission is maximal when the detected area is at the center of the disk, and decreases as the detected area is moved away from the center, showing the extension of the Tamm mode below the disk. As was discussed already for figure 2(a), the emission is directed normal to the sample ($k_x = 0$) for $x = 0$, and leftward (resp. rightward) for the left (resp. right) portion of the sample, with an increase of the emission angle with ΔE corresponding to the $E(k_x)$ parabolic relation. For $\Delta E = 25$ meV, a secondary lobe is observed on the side of the $|x| = 2$ μm emission patterns and well reproduced by theory, we attribute it to the diffraction by the pinhole. The measured emission lobes width at half maximum is of the order of 27° for $|x| = 2$ μm, similar to the simulated value of 22°, and can be assigned to diffraction ; however, this is not the case for $x = 0$: the measured emission pattern is clearly broader than the simulated one, possibly revealing a contribution from direct (not via the Tamm state) nanocrystal emission, which could be higher than simulated due to the lower quality factor of the structure.

Figure 3(b) plots the measured and simulated relation between the emission angle θ (center of the emission lobe) and the detected area position x, for different emission energies. The simulation and experiment are in excellent agreement. On each side of the disk center, the emission direction shows little dependence on the position: $|\theta|$ is a constant as a function of $|x|$ (for $x \neq 0$).

We perform the same analysis for the disk of diameter 4 μm with detection positions of ± 1 μm. For this disk, it was shown in figure 1(c) that the electromagnetic field confinement in the 0D Tamm structure leads to a discretization of the dispersion relation. We plot on figure 4(a) the emission pattern for three different positions on the 4 μm disk, at the energy 1.99 eV of the discretized Tamm mode, and compare it with the simulated patterns (at the theoretical resonant energy 1.91 eV). Again, the $x > 0$ (resp. $x < 0$) portion of the cavity shows a predominance of the $k_x > 0$ (resp. $k_x < 0$) components. These results are in agreement with the simulated electric field distribution of the Tamm cavity mode (figure 4(b)). As discussed now, the non-symmetric emission patterns point to the importance of the complex nature of the complex electric field in the Tamm structure E_x: if

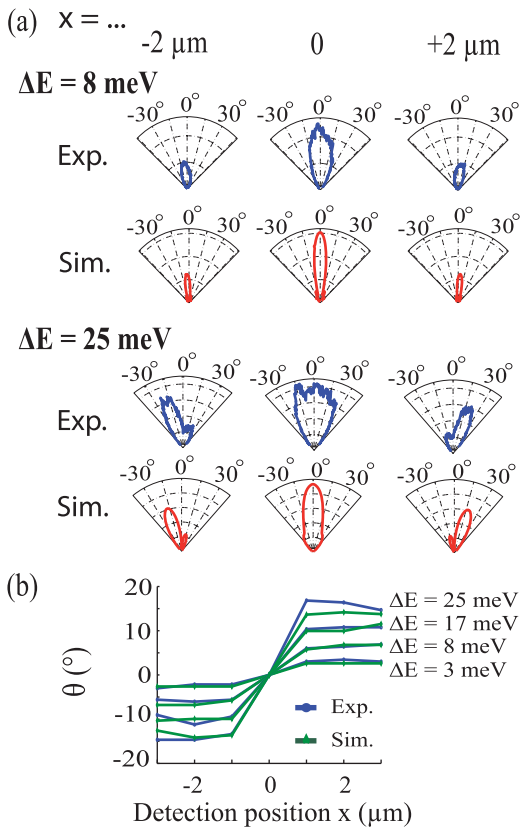

Figure 3. (a) Measured and simulated emission patterns at $\Delta E = 8$ and 25 meV above the fundamental $E(k_x = 0)$, for detection positions $x = -2, 0$ and $+2$ μm on a 10 μm disk. (b) Angle of maximum emission for the simulated and experimental emission patterns, at four energies ΔE, as a function of the detection position x.

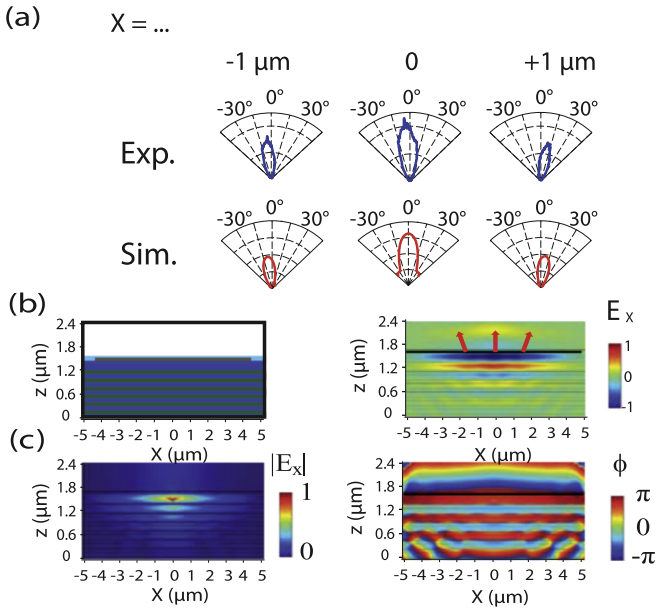

Figure 4. (a) Measured and simulated emission diagram for the confined mode of the 4 μm disk, for three different positions of the detection area. (b) Simulated field distribution E_x for the 4 μm disk resonant mode (4.2 $\times$ 2 μm^2 portion of the total simulation cell size: 20 $\times$ 2.4 μm^2), the black line shows the silver disk. (c) Complex electric field E_x modulus (arb. un.) and argument Φ(rad.) for the same simulation.

E_x was a real number, the emission pattern would be a symmetric function of k_x as it would be the norm of the Fourier transform of a real function of x. Figure 4(c) plots the modulus and argument of E_x inside the 4 μm disk

cavity (while figures 2(b) and 4(b) up to now plotted the real part of E_x). The modulus of E_x shows the localization of the electric field inside the Tamm structure, with emission into the air and substrate. The phase ϕ of E_x, on the other hand, is mostly uniform inside the structure, corresponding to the stationary state (with a π phase at each SiO_2–TiO_2 interface, due to the interface negative reflection coefficient), while it increases monotonously outside the structure, in the air and lower Bragg mirror parts, corresponding to propagating photonic modes.

One notes however that there is, inside the volume of the stationary cavity mode, a slight horizontal phase gradient towards increasing |x|. In a small volume around a point A, $\phi(M) \approx \phi(A) + \overrightarrow{\text{grad}}\,\phi.\,\overrightarrow{AM}$ so that the electric field in this volume can be approximated by a wave of k-vector real part $\overrightarrow{\text{grad}}\,\phi$. This explains why the measurement of the radiation pattern at a detection position x of the structure yields a single lobe centered around a value k_x: this value is equal to the phase gradient $(\partial\phi/\partial x)$. Our measurement scheme thus probes the phase gradient distribution of the Tamm structure mode electric field, which is not accessible by other measurement schemes : for instance, standard fluorescence imaging of the sample provides only the spatial distribution of the modulus of E_x but not its phase, and Fourier analysis without spatial selection by the pinhole (as in figure 1) provides only a combination of all value of k_x. The measured data for the 4 μm disk (figure 4(a)) show that the horizontal phase gradient is directed towards increasing |x|, in agreement with the simulation of figure 4(c). The same is true for the 10 μm disk ; moreover, figure 3(b) shows that the measured phase gradient is uniform (θ is constant) over the $x > 0$ and $x < 0$ portions, in agreement with the simulated curve.

4. Conclusion

In this paper, we analyzed the electric field confined optical modes of 0D-Tamm structures with silver disk diameters ranging from 10 to 2 μm, excited by fluorescent colloidal CdSe/CdS nanocrystals. We performed Fourier-space imaging of the emission for a selected 1.7 μm area of the disk and showed that different detection positions led to different emission patterns (corresponding to different k_x-vector cavity mode distributions), in good agreement with our numerical simulations. In other words, our experiment provided a probe of the phase-gradient distribution of the 0D-Tamm mode electric field. Understanding the relation between the cavity geometry and the spatial and k-vector distribution of its modes is a first step towards the control of the emission direction of nanophotonics structures.

Acknowledgments

This work was funded by the Agence Nationale de la Recherche (project JCJC 12-JS04-0011-01 PONIMI) and the Centre de Compétence Nanosciences Ile-de-France (C'Nano IdF NanoPlasmAA). The authors would like to thank Francis Breton for the setup interface, Loïc Becerra and Stéphane Chenot for sample preparations, Jean-Louis Fave for spectroscopic measurements, and Joël Bellessa and Clémentine Symonds for fruitful discussions.

References

[1] Ahrens T, Burau G K G, Stolz H, Reitzenstein S and Forchel A 2011 Microcavity mode structure investigations with high spatial resolution *Phys. Status Solidi* c **8** 1239
[2] Bonato C, Gudat J, Vries K, Thon S, Kim H, Petroff P, Exter M and Bouwmeester D 2012 Optical modes in oxide-apertured micropillar cavities *Opt. Express* **37** 4678
[3] Ctistis G, Hartsuiker A, Pol E, Claudon J, Vos W and Gérard J M 2010 Optical characterization and selective addressing of the resonant modes of a micropillar cavity with a white light beam *Phys. Rev.* B **82** 195330
[4] Karl M, Li S, Passow T, Loffler W, Kalt H and Hetterich M 2007 Localized and delocalized modes in coupled optical micropillar cavities *Opt. Express* **15** 8191
[5] Gutbrod T, Bayer M and Forchel A 2007 Angle dependence of the spontaneous emission from confined optical modes in photonic dots *Phys. Rev.* B **59** 2223
[6] Rigneault H, Broudic J, Gayral B and Gérard J M 2001 Far-field radiation from quantum boxes located in pillar microcavities *Opt. Express* **26** 8191
[7] Novotny L and Hecht B 2006 *Principles of Nano-Optics* (Cambridge: Cambridge University Press)
[8] Kavokin A V, Shelykh I A and Malpuech G 2005 Lossless interface modes at the boundary between two periodic dielectric structures *Phys. Rev.* B **72** 233102
[9] Kaliteevski M, Iorsh I, Brand S, Abram R A, Chamberlain J M, Kavokin A V and Shelykh I A 2007 Tamm plasmon-polaritons: possible electromagnetic states at the interface of a metal and a dielectric Bragg mirror *Phys. Rev.* B **76** 165415
[10] Badugu R, Descrovi E and Lakowicz J R 2014 Radiative decay engineering 7: Tamm state-coupled emission using a hybrid plasmonic-photonic structure *Anal. Biochem.* **445** 1–13
[11] Frederich H, Wen F, Laverdant J, Coolen L, Schwob C and Maître A 2011 Isotropic broadband absorption by a macroscopic self-organized plasmonic crystal *Opt. Express* **19** 24424
[12] Frederich H, Wen F, Laverdant J, Daney de Marcillac W, Schwob C, Coolen L and Maitre A 2014 Determination of the surface plasmon polariton extraction efficiency from a self-assembled plasmonic crystal *Plasmonics* **9** 917

[13] Gazzano O, Michaelis de Vasconcellos S, Gauthron K, Symonds C, Bloch J, Voisin P, Bellessa J, Lemaitre A and Senellart P 2011 Evidence for confined Tamm plasmon modes under metallic microdisks and application to the control of spontaneous optical emission *Phys. Rev. Lett.* **107** 247402
[14] Gazzano O, Michaelis de Vasconcellos S, Gauthron K, Symonds C, Voisin P, Bellessa J, Lemaitre A and Senellart P 2012 Single photon source using confined Tamm plasmon modes *Appl. Phys. Lett.* **100** 232111
[15] Braun T, Baumann V, Iff O, Höfling S, Schneider C and Kamp M 2015 Enhanced single photon emission from positioned InP/GaInP quantum dots coupled to a confined Tamm-plasmon mode *Appl. Phys. Lett.* **106** 041113
[16] Symonds C, Lheureux G, Hugonin J P, Greffet J J, Laverdant J, Brucoli G, Lemaitre A, Senellart P and Bellessa J 2013 Confined Tamm plasmon lasers *Nano Lett.* **13** 3179
[17] Lheureux G, Azzini S, Symonds C, Senellart P, Lemaître A, Sauvan C, Hugonin J-P, Greffet J-J and Bellessa J 2015 Polarization-controlled confined Tamm plasmon lasers *ACS Photon.* **2** 842
[18] Leosson K, Shayestehaminzadeh S, Tryggvason T K, Kossoy A, Agnarsson B, Magnus F, Olafsson S, Gudmundsson J T, Magnusson E B and Shelykh I A 2012 Comparing resonant photon tunneling via cavity modes and Tamm plasmon polariton modes in metal-coated Bragg mirrors *Opt. Lett.* **37** 4026
Lopez-Garcia M, Ho Y-L D, Taverne M P C, Chen L-F, Murshidy M M, Edwards A P, Serry M Y, Adawi A M, Rarity J G and Oulton R 2014 Efficient out-coupling and beaming of Tamm optical states via surface plasmon polariton excitation *Appl. Phys. Lett.* **104** 231116
[19] Zhang X L, Song J F, Li X B, Feng J and Sun H B 2012 Optical Tamm states enhanced broad-band absorption of organic solar cells *Appl. Phys. Lett.* **101** 243901
[20] Mahler B, Spinicelli P, Buil S, Quelin X, Hermier J-P and Dubertret B 2008 Towards non-blinking colloidal quantum dots *Nat. Mater.* **7** 659